Earth and Planetary Science Letters 274 (2008) 59–71

Contents lists available at ScienceDirect

Earth and Planetary Science Letters

journal homepage: www.elsevier.com/locate/epsl

Age calibrated relative paleointensity for the last 1.5 Myr at IODP Site U1308 (North Atlantic)

J.E.T. Channell [a,*], D.A. Hodell [a,1], C. Xuan [a], A. Mazaud [b], J.S. Stoner [c]

[a] Department of Geological Sciences, University of Florida, 241 Williamson Hall, Gainesville, FL 32611, USA
[b] Laboratoire des Sciences du Climat et de l'Environnement, CEA-CNRS, 91198 Gif-sur-Yvette France
[c] College of Oceanic and Atmospheric Sciences, Oregon State University, Corvallis, OR 97331, USA

ARTICLE INFO

Article history:
Received 26 March 2008
Received in revised form 1 July 2008
Accepted 1 July 2008
Available online 15 July 2008

Editor: P. DeMenocal

Keywords:
geomagnetic paleointensity
oxygen isotope stratigraphy
Quaternary
signal correlation

ABSTRACT

Integrated Ocean Drilling Program (IODP) Site U1308 (central North Atlantic) records paleomagnetic directional and relative paleointensity (RPI) variations for the last 1.5 Myr, in 110 m of the sediment sequence at a mean sedimentation rate of 7.3 cm/kyr. A detailed benthic oxygen isotope record was combined with RPI to produce an integrated, high-resolution magneto-isotopic stratigraphy for Site U1308. Apart from the well-known polarity reversals in this interval, the Punaruu excursion is recorded at 1092 ka and the Cobb Mountain Subchron in the 1182–1208 ka interval. The paleointensity proxies are determined as slopes of NRM versus ARM and NRM versus ARMAQ (ARM acquisition) with linear correlation coefficients to monitor the quality of the linear fit. The RPI record for Site U1308 is compared with the three other paleointensity records (one from the Western Equatorial Pacific and two from the North Atlantic) that cover the same time interval and have accompanying oxygen isotope records. The Match protocol of Lisiecki and Lisiecki (2002) [Lisiecki, L. E. and P. A. Lisiecki, The application of dynamic programming to the correlation of paleoclimate records, Paleoceanography, 17(D4), 1049, doi:10.1029/2001PA000733, 2002] is used to optimize the correlation of paleointensity records. Beginning with the original (published) age models for each record, the Match routine is used to optimize the RPI correlations to Site U1308, with checks to ensure compatibility with oxygen isotope records. Squared wavelet coherence (WTC) indicates significant improvement in RPI (and oxygen isotope) correlations after matching each RPI record to Site U1308, particularly for periods >10 kyr. The level of coherence for the Atlantic RPI records and the lower resolution Pacific record implies synchronous global variability (at scales >10 kyr) that can be attributed to the axial dipole geomagnetic field.

1. Introduction

Integrated Ocean Drilling Program (IODP) Site U1308 (Fig. 1) was drilled in November 2004, during IODP Expedition 303. The site constitutes a reoccupation of Deep Sea Drilling Project (DSDP) Site 609 that was drilled in 1983 during DSDP Leg 94. The marly foraminiferal nannofossil ooze at this site exhibits distinctive varicolored glacial–interglacial cycles in the Brunhes and Matuyama Chronozones, excellent preservation of calcareous and siliceous microfossils, and the necessary attributes for generation of high-resolution isotopic and paleointensity-based chronostratigraphies. Sites 607 and 609, both drilled during DSDP Leg 94, have been very important for generating benthic $\delta^{18}O$, $\delta^{13}C$ and $CaCO_3$ records for the Pleistocene (Ruddiman et al., 1989) and late Pliocene (Ruddiman et al., 1986; Raymo et al., 1989) and interpreting these records in terms of ice sheet variability and oceanic circulation changes, and for generating orbitally tuned timescales. The importance of DSDP Site 609 was accentuated by recognition of detrital (Heinrich) layers, deposited by massive iceberg discharges from Hudson Strait (Bond et al., 1993; Bond and Lotti, 1995). Partly from petrologic characteristics observed at DSDP Site 609, Heinrich Events were found to be superimposed on another, higher-frequency rhythm of ice rafting events with approximately 1500-year pacing (Bond et al., 1999; Bond et al., 1997).

These millennial-scale climatic events, observed at DSDP Site 609 and elsewhere in the North Atlantic, have been correlated with Greenland ice core $\delta^{18}O$ records, and with paleoclimate proxy records from the Santa Barbara Basin, Arabian Sea, Cariaco Basin and China, although the phasing, causes, and linkages among these various regions remain uncertain. Indeed, long-distance correlations, based on matching of climate records, often pre-suppose synchronicity for which there is no independent evidence (see Wunsch, 2006). Studies of past climate change are challenged by the need for long-distance correlation at an appropriate resolution for discerning subtle phasing (leads and lags) in the climate system. Coupled relative paleointensity (RPI) and oxygen isotope records may provide a level of stratigraphic resolution that cannot be matched by oxygen isotope stratigraphy alone; however, uncertainties remain about the scale at which RPI

* Corresponding author. Tel.: +1 352 392 3658; fax: +1 352 392 9294.
E-mail address: jetc@geology.ufl.edu (J.E.T. Channell).
[1] Current address: Godwin Laboratory for Paleoclimate Research, Department of Earth Sciences, University of Cambridge, Downing Street, Cambridge, CB2 3EQ, United Kingdom.

0012-821X/$ – see front matter © 2008 Elsevier B.V. All rights reserved.
doi:10.1016/j.epsl.2008.07.005

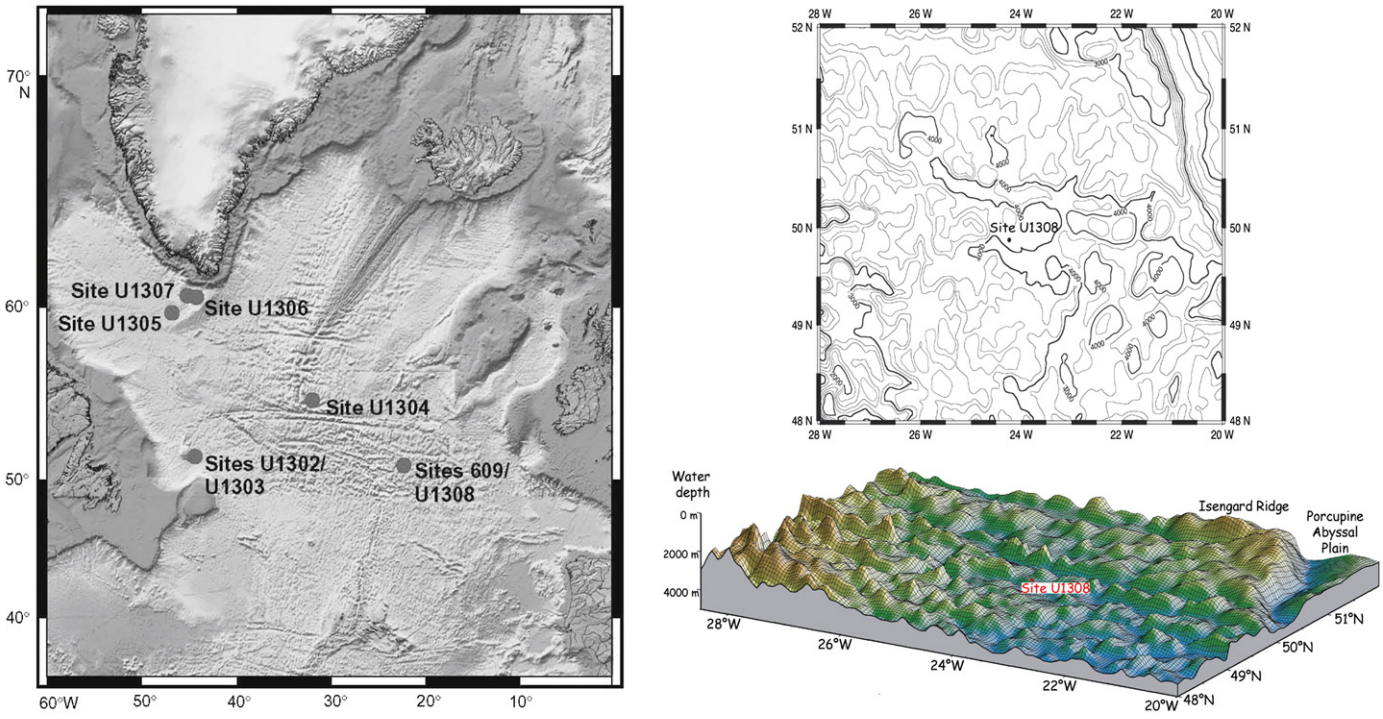

Fig. 1. Location of IODP Site U1308 (re-drill of DSDP Site 609) and other sites occupied during IODP Expedition 303.

records can be globally correlated. For example, is effective correlation restricted to RPI minima associated with excursions and reversals, or can global correlations be achieved at millennial or centennial scale? The emphasis in this paper is on stratigraphy because establishing the stratigraphy is a necessary first step for making the paleomagnetic data useful for ground-truthing numerical simulations of the geomagnetic field, as well as for answering fundamental geophysical questions. For instance, do secular variations, excursions and brief subchrons constitute part of a continuum of geomagnetic behavior with polarity chrons? Are the characteristics of secular variation different for the two polarity states, and are polarity transition fields comparable for sequential polarity reversals? As geomagnetic field intensity is a control on cosmogenic nuclide production, does the apparent correlation of the 1500-yr cycle in North Atlantic IRD to cosmogenic isotope production (Bond et al., 2001) imply a link between climate and geomagnetic field strength (and/or between climate and solar activity)? Do the presence of orbital periods in RPI data support a primary climate/paleointensity connection or do they denote climate-related contamination of RPI records?

In this paper, we report the Site U1308 paleomagnetic record for the last 1.5 My, corresponding to the 0–110 meters composite depth (mcd) interval for which an oxygen isotope stratigraphy is available (Hodell et al., submitted for publication). U-channel samples (samples enclosed in plastic containers with a 2×2 cm cross-section and the same length as the core section, usually 150 cm) were collected from the archive half of each core section within the composite splice (Hodell et al., submitted for publication; Expedition 303 Scientists, 2006). One of the sides of the u-channel comprises a clip-on plastic lid that allows the sample to be sealed to inhibit dehydration and other chemical/physical changes. Samples (10 cc) for stable isotope analyses were collected at 2 cm intervals from the working half of the same composite splice. Oxygen isotope analyses were measured on the benthic foraminifer *Cibicidoides wuellerstorfi* and/or *Cibicidoides kullenbergi* at a sample spacing of 2-cm for the upper 110 mcd. Specimens were picked from the >212-μm size fraction, and one to five individuals were used for $\delta^{18}O$ analysis yielding a total of almost 5000 data points (Hodell et al., in review).

2. Magnetic properties and methods

Natural remanent magnetization (NRM) of u-channel samples was measured at 1-cm spacing before demagnetization, and after 12 demagnetization steps in the 20–100 mT peak field range, using a 2G Enterprises cryogenic magnetometer designed to measure u-channel samples. Shipboard AF treatment of archive halves of core sections (from which the u-channels were collected post-cruise) was carried out at peak fields not exceeding 10 mT (Expedition 303 Scientists, 2006). The response functions of the three orthogonal pick-up coils of the u-channel magnetometer have a width at half-height of ~4.5 cm (Weeks et al., 1993; Guyodo et al., 2002), therefore, measurements at 1-cm spacing are not independent from one another. Component magnetization directions were computed for NRM data at 1-cm spacing using the standard "principal component" method (Kirschvink, 1980). The demagnetization interval used to compute the characteristic magnetization component was 20–80 mT, and the maximum angular deviation (MAD) values provide a means of monitoring the uncertainty associated with component magnetization directions. Susceptibility measurements of u-channel samples were carried out using a susceptibility track with a pick-up loop that has a response function similar to that of the u-channel magnetometer used for remanence measurements (Thomas et al., 2003). For each u-channel, anhysteretic remanent magnetization (ARM) was acquired in a peak alternating field of 100 mT and a 50 μT DC bias field. ARM was measured prior to demagnetization and then after demagnetization at the same demagnetization steps used for NRM, up to peak fields of 60 mT. The samples were then demagnetized at peak fields of 105 mT, and ARM was reacquired stepwise in peak alternating fields of 20–60 mT, in 5 mT steps, and a constant 50 μT DC bias field.

The high fidelity of the oxygen isotope record (Fig. 2a) for the upper 110 mcd at Site U1308 permits unambiguous identification of

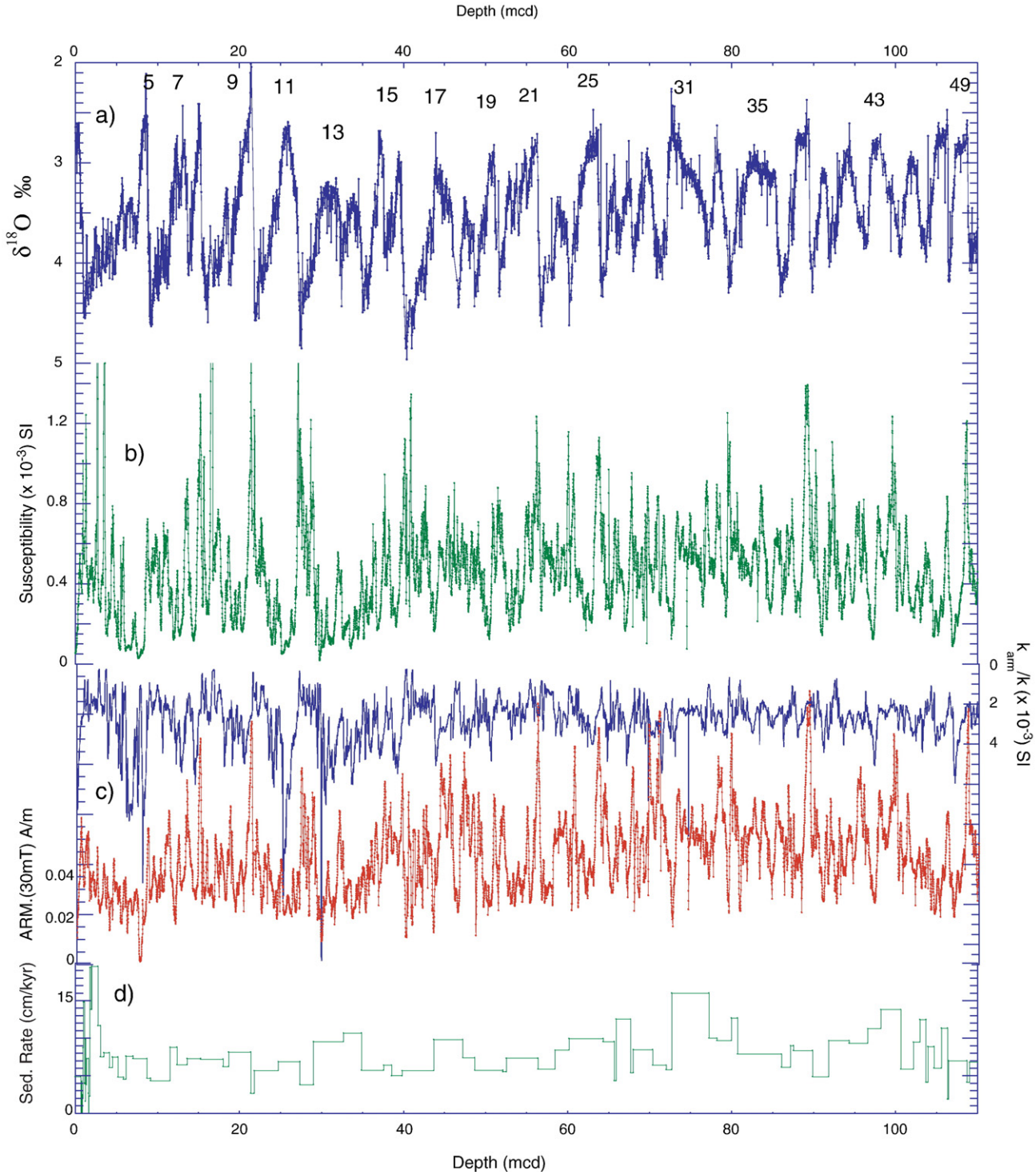

Fig. 2. (a) Benthic oxygen isotope record (Hodell et al., submitted for publication) with marine oxygen isotope stages, (b) Volume magnetic susceptibility, (c) Anhysteretic susceptibility divided by susceptibility (karm/k) and anhysteretic magnetization (ARM) intensity after demagnetization at peak fields of 30 mT, (d) Interval mean sedimentation rates from the fit of the oxygen isotope record to the reference curve.

isotope stages to marine isotope stage (MIS) 50 at 1.5 Ma (Hodell et al., submitted for publication). Low field susceptibility (Fig. 2b) varies with glacial–interglacial cycles, with low values corresponding to interglacial stages reflecting biogenic carbonate dilution of magnetic concentration, and reduced concentration of susceptible ice-rafted debris (IRD). Susceptibility peaks during MIS 3 correspond to Heinrich layers 1, 2, 4 and 5, and peaks associated with earlier glacial stages and Terminations are also associated with Heinrich-type IRD layers (Hodell et al., submitted for publication). ARM intensity (Fig. 2c) tends to mimic susceptibility although, as expected, it is less sensitive than susceptibility to the coarse detritus associated with IRD-rich layers. The magnetite grain size proxy, karm/k (Fig. 2c), the ratio of anhysteretic susceptibility (ARM intensity divided by the ARM bias field) to susceptibility, yields low values corresponding to susceptibility peaks, indicative of coarser grained magnetite, and high values indicative of relatively fine-grained magnetite corresponding to minima in susceptibility and ARM.

The age model for the upper 110 mcd at Site U1308 (Hodell et al., submitted for publication) was based on the optimal fit of the benthic

oxygen isotope record to the oxygen isotope stack of Lisiecki and Raymo (2005), augmented by correlations to Core MD952042 (Shackleton et al., 2004) for the 35–60 ka interval, and by ^{14}C ages in the 14–35 ka interval that were transferred from Site 609 using reflectance records (Hodell et al., submitted for publication). The resulting sedimentation rate map (Fig. 2d) indicates interval sedimentation rates in the range of 3.8–16.0 cm/kyr, with minima in glacial stages MIS 10, 12 and 48, and the maximum in interglacial stage MIS 31. Although other interglacial stages, such as MIS 13 and MIS 17, have relatively high sedimentation rates, other prominent interglacial stages such as MIS 11 do not have particularly elevated sedimentation rates relative to neighboring glacial intervals.

The AF demagnetization characteristics of the NRM indicate a low-coercivity remanence carrier, probably magnetite. A plot of anhysteretic susceptibility versus susceptibility can be used to estimate the grain size distribution of magnetite and, according to the calibration of King et al. (1983), the magnetite at Site U1308 is largely in grain sizes close to 1 μm (Fig. 3a). Samples that plot in the field associated with grain sizes greater than 5 μm (Fig. 3a) are all associated with thin Heinrich-like IRD layers denoted by susceptibility peaks (Fig. 2b). Hysteresis ratios from the background sediments outside the detrital layers, measured using a Princeton Measurements Corp. vibrating sample magnetometer (VSM), lie in the pseudo-single domain (PSD) field of the Day et al. (1977) hysteresis ratio plot (Fig. 3b) and trace a typical magnetite grain size mixing curve between single-domain (SD) and multi-domain (MD) grains.

3. Natural Remanent Magnetization (NRM)

NRM components were determined for the 20–80 mT peak field demagnetization interval (12 steps), using the standard three-dimensional least squares protocol (Kirschvink, 1980), without anchoring the fit to the origin of orthogonal projections. The maximum peak demagnetization field (100 mT) reduced the NRM to about 5% or less of the NRM intensity prior to u-channel demagnetization, indicating a dominate low-coercivity magnetization and no clear evidence for high-coercivity NRM carriers. The maximum angular deviation (MAD) values associated with the component magnetization directions, computed at 1-cm intervals, are generally below 5° indicative of well-defined magnetization components (Fig. 4c). MAD values could be reduced in some intervals by choosing a modified demagnetization interval rather than the global (20–80 mT) interval. We prefer to plot the component directions and MAD values for the global (20–80 mT) demagnetization interval, as this allows a more straightforward assessment of the quality of the directional record down-core (Fig. 4). Declinations were corrected core orientation using the "tensor" core orientation data, where available (light blue symbols in Fig. 4b), and by rotation of entire cores so that the mean declination is oriented North or South for positive and negative inclination intervals, respectively (dark blue symbols inFig. 4b). The differences between the declination values determined using these two methods indicate that the "tensor" tool is not always a reliable means of core orientation. Nonetheless, the declination and inclination data, placed on the oxygen isotope age model (Fig. 4), are readily correlated to the geomagnetic polarity timescale (GPTS) with the addition of an event that we interpret as correlating with the Punaruu polarity excursion. This excursion appears in 3 of 5 holes in the shipboard data (Expedition 303 Scientists, 2006), and is represented in the composite section (Fig. 4) by more than 12 individual component magnetizations. Its appearance is due to the high mean sedimentation rate (16 cm/kyr) in this interval representing the transition from MIS 32 to MIS 31 (Fig. 2d). NRM intensities before AF demagnetization and after AF treatment at two peak fields (30 and 50 mT) indicate minima associated with polarity reversals and the Punaruu excursion (Fig. 4d).

The Punaruu excursion originates from the Punaruu Valley (Tahiti) where normal polarity magnetizations were recorded in basaltic lava flows stratigraphically below, and distinct from, the Jaramillo Subchronozone (Chauvin et al., 1990). The Punaruu excursion in the type section on Tahiti has yielded an age of 1105 ka using $^{40}Ar/^{39}Ar$ methods (Singer et al., 1999). This excursion appears in the sediment record from ODP Site 1021 (California Margin) where an age of 1.1 Ma is based on assumed uniform sedimentation rate between the M/B

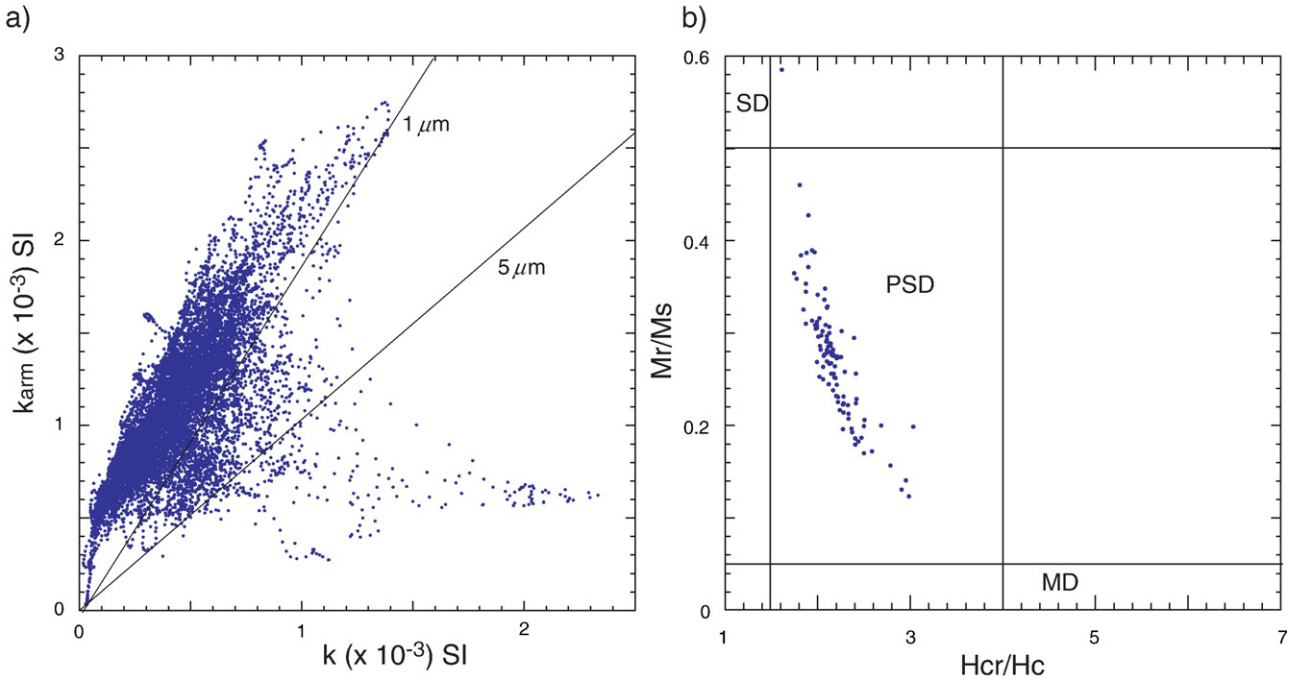

Fig. 3. (a) Anhysteretic susceptibility (k_{arm}) plotted against volume susceptibility (k). Grain size estimates for magnetite from King et al. (1983). (b) Hysteresis ratios lying in the pseudo-single domain (PSD) field, along a magnetite mixing line between single domain (SD) and multi-domain (MD) fields with of Day et al. (1977).

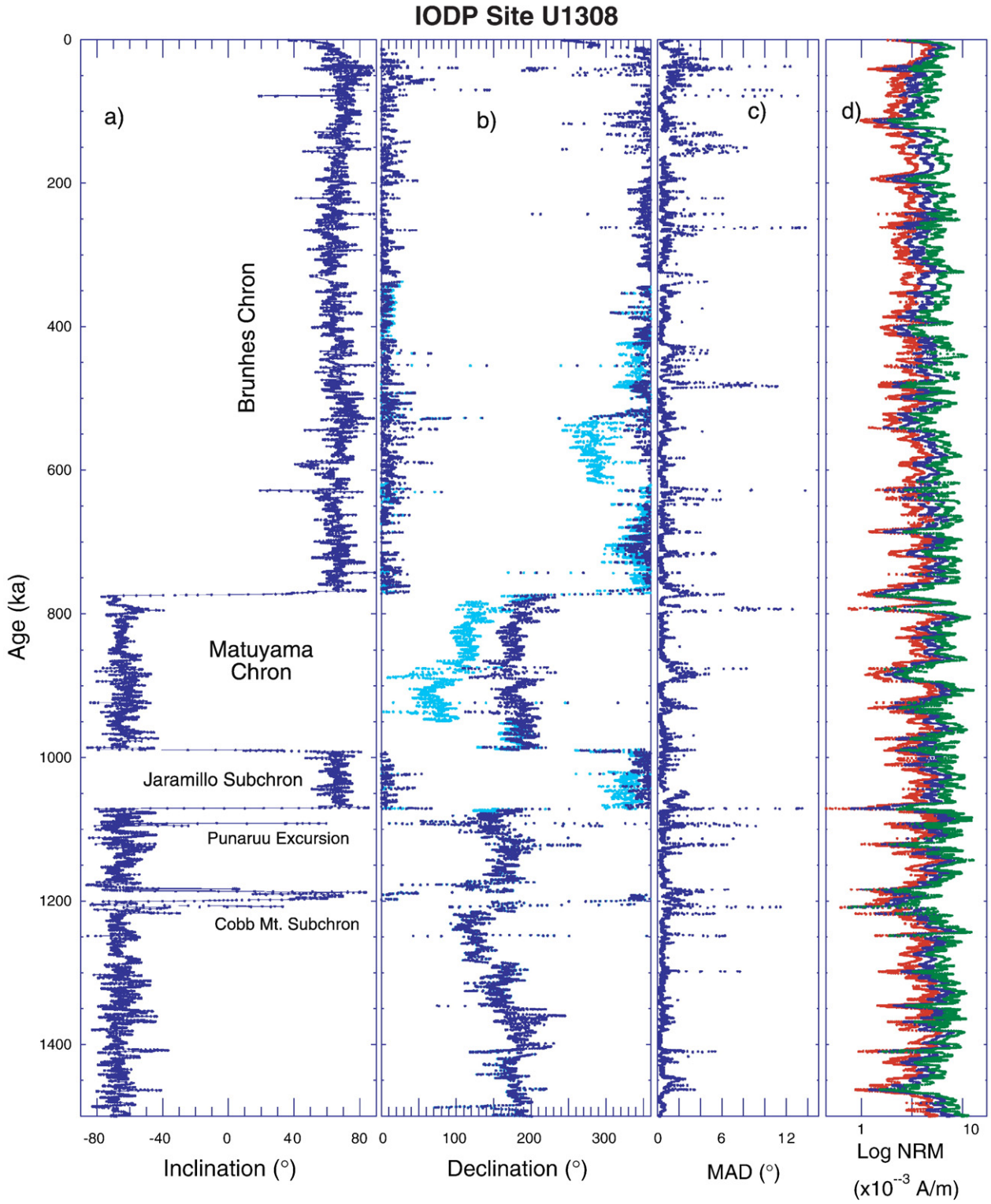

Fig. 4. Natural remanent magnetization (NRM) components determined in the 20–80 mT peak field demagnetization interval, (a) inclination, (b) declinations rotated using uniform rotations for each core (dark blue) and tensor core orientation data where available (light blue), (c) maximum angular deviation (MAD) values, (d) NRM intensities prior to AF demagnetization (green), after demagnetization at peak fields of 30 mT (blue) and 50 mT (red).

boundary and the top of the Jaramillo Subchronozone (Guyodo et al., 1999). At both ODP Sites 983 and 984, the same excursion was interpreted to occur at 1115 ka (Channell et al., 2002). The quality and resolution of the oxygen isotope record at Site U1308 is considerably higher than at Sites 983/984 in this interval, due in part to the paucity of foraminifera at Sites 983/984. At Site U1308, the Punaruu excursion occurs within MIS 32 at 1092 ka and has an estimated duration of about 1 kyr.

Mankinen et al. (1978) documented a normal polarity site in the Alder Creek rhyolite at Cobb Mountain (California) which has yielded an $^{40}Ar/$

^{39}Ar age of 1186 ka (Turrin et al., 1994). Further work by Mankinen and Grommé (1982) in the Coso Range (California) supported the existence of the Cobb Mountain "Event". DSDP Site 609 provided the first unequivocal documentation of a normal polarity zone of this age in deep-sea sediments (Clement and Kent, 1987; Clement and Martinson, 1992). At Site 609, the so-called Cobb Mountain Subchron can be correlated to MIS 35/36 (Ruddiman et al., 1989). At ODP Sites 980 and 983/984, it correlates to MIS 35–37 at ~1.2 Ma and has an estimated duration of 35 kyr (Channell et al., 2002; Channell and Raymo, 2003). The duration estimate for the Cobb Mt. Subchron at Site U1308 (26 kyr) is less than that from ODP Sites 980 and 983/984, although the top and base of the subchron are correlated to the same marine isotope stages as at Sites 980 and 983/984.

4. Relative Paleointensity (RPI) determinations

The detrital remanent magnetization of sediments depends on the intensity of the geomagnetic field, and the concentration and alignment efficiency of remanence-carrying grains. In favorable circumstances, the relative strength of the magnetizing field can be determined

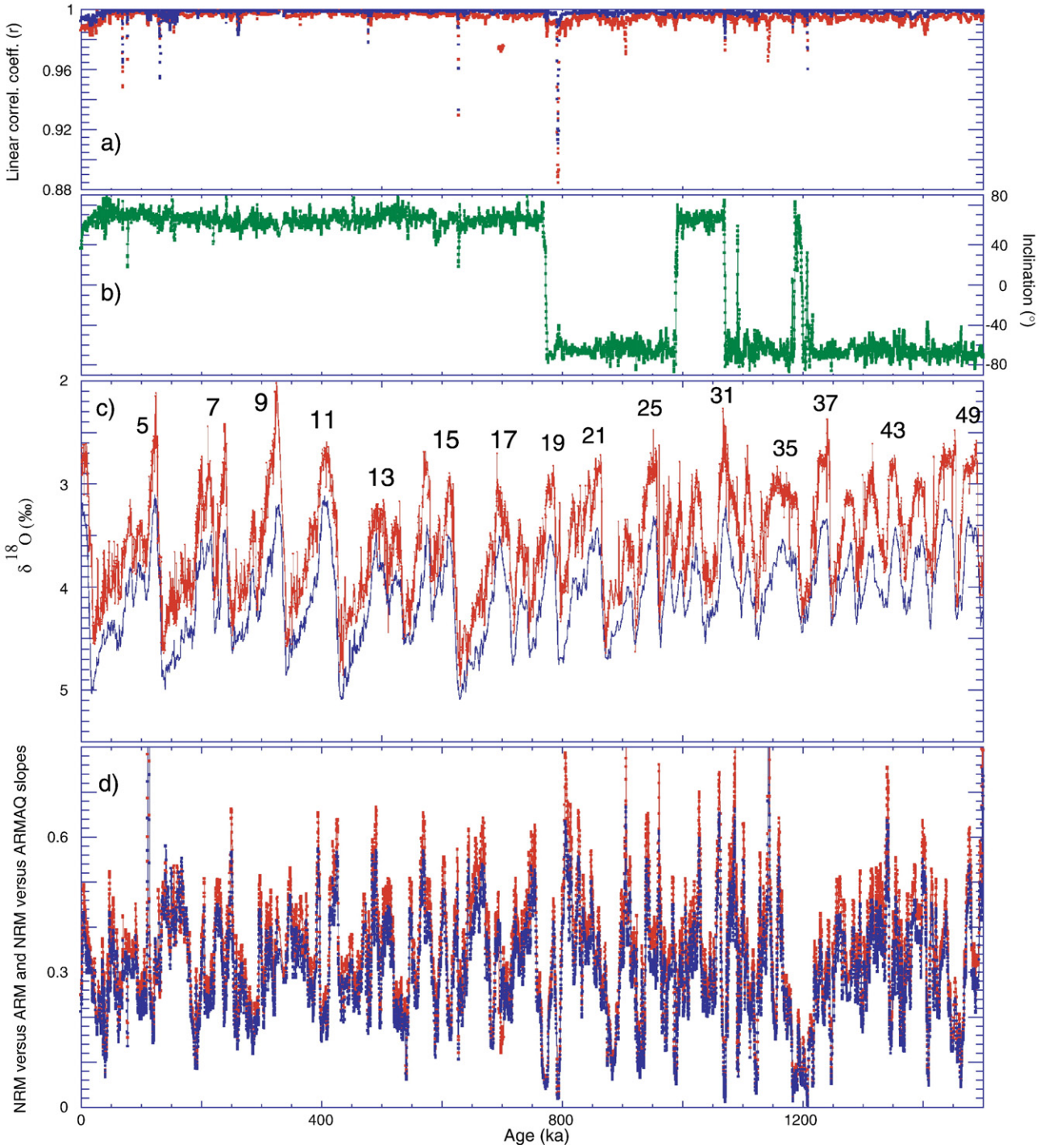

Fig. 5. (a) Linear correlation coefficients for slopes of NRM versus ARM (red) and NRM versus ARMAQ (blue), (b) component inclination of NRM from Fig. 4, (c) benthic isotope record (red) correlated to the reference stack (Lisiecki and Raymo, 2005) (blue), (d) Slopes of NRM versus ARM and NRM versus ARMAQ for the 20–60 mT demagnetization and acquisition interval.

by using the intensity of different types of laboratory-induced magnetizations (ARM and IRM) to normalize the NRM for changes in concentration of remanence-carrying grains. The resulting normalized remanence can be a proxy for relative paleointensity (RPI) variations (King et al., 1983; Banerjee and Mellema, 1974; Levi and Banerjee, 1976; Tauxe, 1993). Progress has been accelerated by the development of the small access long-core "u-channel" magnetometer (Weeks et al., 1993) and the u-channel sampling method (Tauxe et al., 1983), which make these high-resolution studies a practical undertaking.

Our procedure for determining RPI proxies is to calculate two slopes: the slopes of NRM-lost versus ARM-lost and ARMAQ (ARM acquisition) over specific demagnetization (acquisition) intervals. These two slopes are similar to calculating the NRM/ARM and NRM/ARMAQ ratios, and are accompanied by linear correlation coefficients (r) that yield the quality of linear fit of each slope, calculated at 1-cm intervals down-core see (Channell et al., 2002). In Fig. 5, we plot slopes of NRM versus ARM and NRM versus ARMAQ and associated r-values for the 20–60 mT peak field demagnetization/acquisition interval. The two proxies are almost identical, and linear correlation coefficient (r) values are close to unity. A prominent departure from unity for both NRM/ARM and NRM/ARMAQ occurs in MIS 20 associated with the low in paleointensity that occurs just prior to the Matuyama–Brunhes boundary.

5. Correlation of RPI records using dynamic programming

We compare the Site U1308 relative paleointensity (RPI) record (slope of NRM versus ARM) with the published RPI stack for the Brunhes Chron (Sint-800) (Guyodo and Valet, 1999), the more recently published Sint-2000 stack (Valet et al., 2005), the EPAPIS stack from the Pacific (Yamazaki and Oda, 2005), the well-calibrated RPI from equatorial Pacific (Valet and Meynadier, 1993), and the inversion from the East Pacific Rise marine magnetic anomaly data (Gee et al., 2000) (Fig. 6). The comparison indicates that the records are rather consistent at timescales of 10^5 years, but much less compatible at scales of 10^4 years. Inconsistencies of RPI at finer time scales may be the result of variable resolution (sedimentation rate), inadequate age control for individual records, or lithologic influences. In addition, smoothing inherent in the creation of the Sint and EPAPIS stacks at 10^4-yr scales (Guyodo and Valet, 1999; Valet et al., 2005; Yamazaki and Oda, 2005) and relatively low sedimentation rates in the equatorial Pacific record (Valet and Meynadier, 1993) may contribute to poor correlation at shorter time scales.

We now compare the Site U1308 paleointensity (RPI) record (slope of NRM/ARM) with other individual records that cover the same interval (i.e., 1.5 Myr), and have accompanying oxygen isotope records. These conditions are limited to three records: ODP Sites 983 and 984 from the Iceland Basin (Channell et al., 1997, 1998, 2004; Channell, 1999; Channell and Kleiven, 2000) and the western Pacific record (Core MD972143) ofHorng et al. (2002, 2003). When these three records are placed on their published isotope age models, and compared with Site U1308, discrepancies both in isotope correlations and RPI correlations are apparent (Supplementary materials: Figs. 1 and 2), and may be attributed to the use of different isotope reference curves to construct the (published) isotopic age models, and other uncertainties inherent in the stable isotope age models. For example, in the 410–430 ka interval, the discrepancy in the apparent age of Termination V for Sites 983/984 and Site U1308/MD972143 (Supplementary materials: Fig. 1) is due to the difference between the Lisiecki and Raymo (2005) isotope stack (used as the reference for Site U1308) and

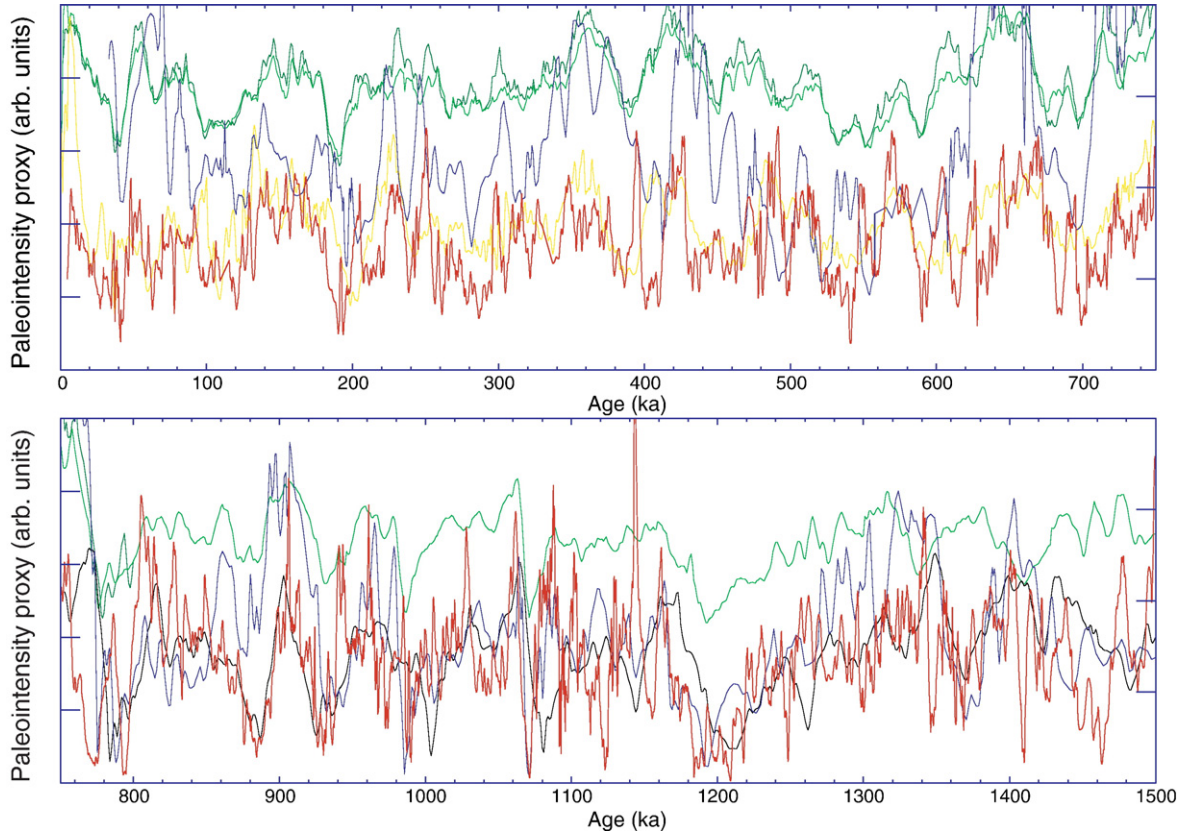

Fig. 6. Relative paleointensity (RPI) record for Site U1308 (red) compared to the Sint-800 (dark green) and Sint-2000 (light green) RPI stacks (Guyodo and Valet, 1999; Valet et al., 2005), equatorial Pacific RPI records from ODP Leg 138 sites (blue) (Valet and Meynadier, 1993), the EPAPIS Pacific RPI stack (black) (Yamazaki and Oda, 2005), the paleointensity inversion of the East Pacific Rise marine magnetic anomaly data (yellow) (Gee et al., 2000).

a previous isotopic reference curve used for Sites 983/984. Discrepancies in RPI records, placed on their original (published) age models, are particularly marked in the 550–950 ka interval (Supplementary materials: Figs. 2).

In order to optimize the correlation of RPI records, we use the "Match" protocol (Lisiecki and Lisiecki, 2002), which utilizes dynamic programming, to compare possible alignments of two records to find a globally optimal alignment. Compared with previous attempts to automate signal correlation (e.g. Martinson et al., 1982), the algorithm requires no initial guess and is less susceptible to finding local solutions. The protocol was applied to 57 oxygen isotope records by Lisiecki and Raymo (2005) to construct their benthic oxygen isotope, which serves as the current benthic isotope (ice volume) template. All RPI records were normalized to have a mean of 0 and a standard deviation of 1 before matching. The dynamic programming algorithm divides each time series into designated intervals and calculates an alignment score for possible mapping of each interval between record pairs. Sequential ordering of these intervals avoids negative derivatives of the matching function. The process allows penalty functions that limit sedimentation rate changes within records, and the range of relative extension/compression between record pairs can be stipulated. The protocol ensures matching of neighboring intervals, and can impose "hard" tie-points (e.g. Terminations in the oxygen isotope records). The number of intervals (750 in our case), into which the time series is divided controls the scale at which the sedimentation rate is allowed to vary, and therefore sets the maximum resolution of the correlation (2 kyr in our case).

The matching process began with the published (oxygen isotope) age models for Sites 983 and 984, and Core MD972143 (Supplementary materials: Figs. 1 and 2). We then applied the minimum number of hard isotope tie-points that allows the Match protocol to achieve the optimal RPI match (Fig. 7), consistent with isotope records placed on the same adjusted age model (Fig. 8). In view of the inconsistent correlation of Termination V at 410–430 ka for Sites 983 and 984 (Supplementary materials: Fig.1), we apply a "hard" tie-point to anchor all three records to an acceptable age (428 ka) for Termination V, consistent with Site U1308 age model. In addition, we found it necessary to impose one additional tie-point at Termination VII (622 ka) for ODP Site 984, two tie-points at 108 ka and 130 ka for Site 983, and eight additional tie-points for Core MD972143 at 336 ka (Termination IV), 867 ka (Termination X), 1060 ka, 1118 ka, 1123 ka, 1193 ka, 1245 ka and 1341 ka. Core MD972143 has the lowest resolution (sedimentation rate) of the four records, and required six hard tie-points in the 1060–1352 ka interval to optimally correlate the RPI and isotope records to IODP Site U1308. In this interval, there were large offsets of the Core MD972143 isotope record, on its original age model, with the isotopic template (Lisiecki and Raymo, 2005) used for calibration of Site U1308, which could not be adequately overcome by the Match protocol applied to RPI. The optimal RPI correlation that is consistent with the oxygen isotope data can be achieved by introducing 2, 3 and 9 isotopic tie-points for Site 984, Site 983 and Core MD972143, respectively.

The Site U1308 sedimentary record for the last 1.5 Myr has a mean sedimentation rate of 7.3 cm/kyr. The Site U1308 mean sedimentation rate is about three times that for Core MD972143, and about half those at ODP Sites 983 and 984 (Supplementary materials: Fig. 3). The matching procedure modifies the mean sedimentation rate between tie-points in the original (published) age models without introducing unreasonable variability (Supplementary materials: Fig. 3). Although

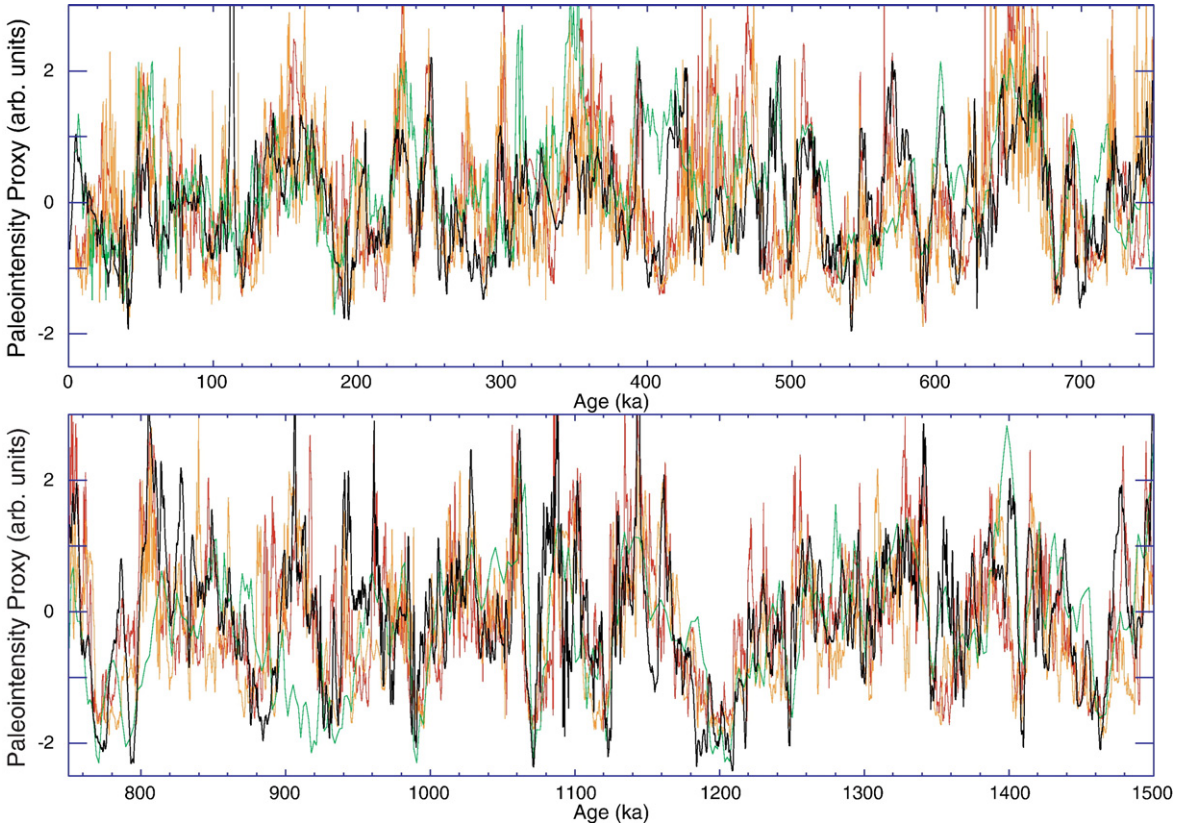

Fig. 7. Relative paleointensity (RPI) record for Site U1308 (black) compared to the RPI records from ODP Sites 983 (red) and 984 (orange) (see text for references), and from Core MD972143 (light green) (Horng et al., 2002, 2003) on their optimal (adjusted) age models based on RPI and isotope data and the Match protocol (Lisiecki and Lisiecki, 2002), where Site U1308 provides the reference RPI record.

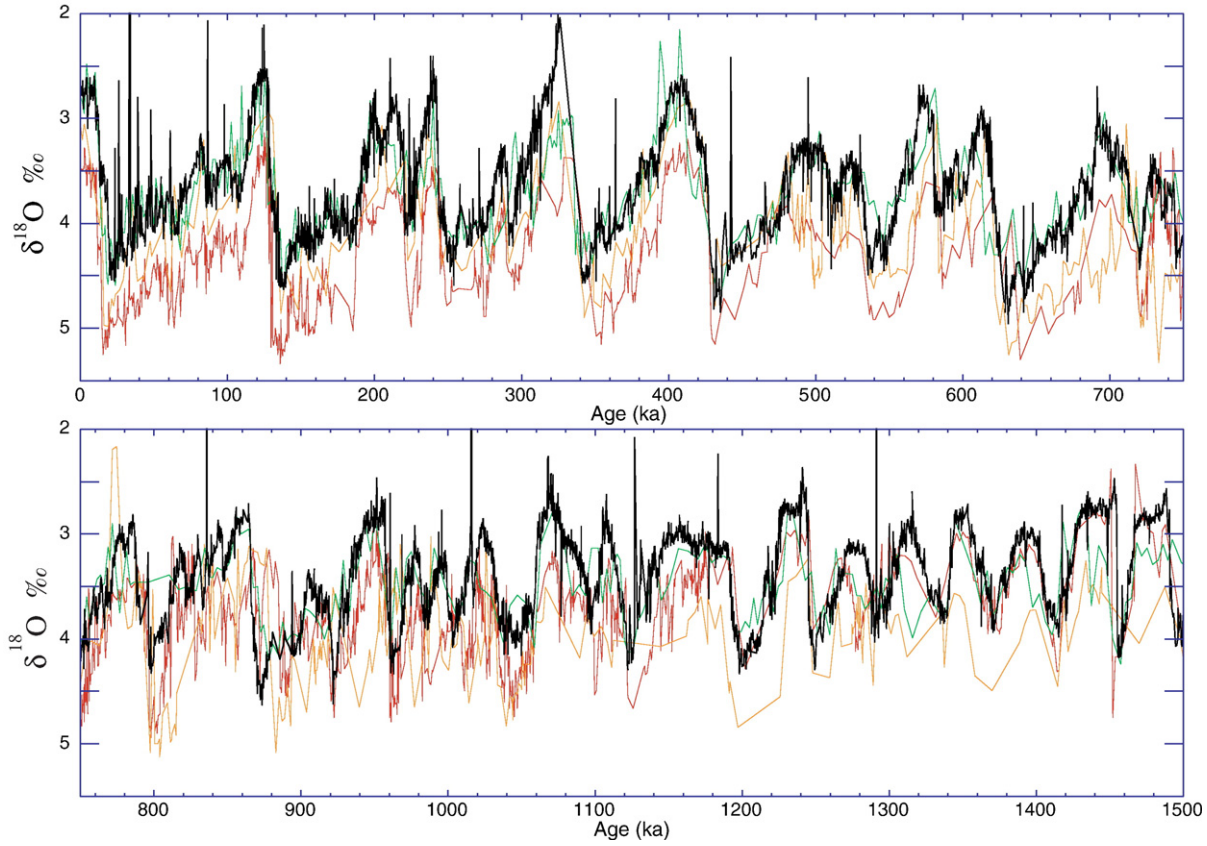

Fig. 8. Benthic oxygen isotope records for Site U1308 (black) compared to benthic oxygen isotope records from ODP Sites 983 (red) and 984 (orange) (see text for references), and from Core MD972143 (light green) (Horng et al., 2002, 2003) on their optimal (adjusted) age models based on relative paleointensity (RPI) and isotope data and the Match protocol (Lisiecki and Lisiecki, 2002), where Site U1308 provides the reference RPI record.

the Site U1308 record does not have the highest potential resolution among the records that we compare, the Site U1308 benthic oxygen isotope record has greater resolution than for most of the Site 983 or Site 984 record (Fig. 8), due in part to the low abundance of foraminifera prior to 1050 ka at Sites 983/984. In view of the superior oxygen isotope stratigraphy for Site U1308, this record is used as the reference record, and the Match protocol is used to correlate the other RPI records to the Site U1308 record, while ensuring that the resulting correlations do not violate correlations of Terminations in the oxygen isotope records. This procedure of reconciling paleointensity and oxygen isotope records is more objective and better constrained than visual matching, can be repeated, and represents a way forward in integrating paleointensity and oxygen isotope stratigraphies.

To test whether the 'matching' process has indeed improved the correlation between the Site U1308 record and other RPI records, we calculate the squared wavelet coherence (WTC) before and after matching. The definition of the WTC resembles that of a traditional correlation coefficient, and can be thought of as a localized correlation coefficient in time-frequency space. Compared with traditional coherence analysis, which reveals the phase relationship and coherency between two signals within particular frequency bands (in the frequency domain), squared wavelet coherence is a more powerful method for testing proposed linkages between two time series (Grinsted et al., 2004; Torrence and Compo, 1998; Torrence and Webster, 1999). It can be used to identify both frequency bands and time intervals within which the two time series are co-varying (Torrence and Webster, 1999; Liu, 1994). The statistical significance level of the squared wavelet coherence is estimated using Monte Carlo methods (Grinsted et al., 2004; Torrence and Compo, 1998). The RPI values were linearly interpolated at 1 kyr increments prior to calculation of the squared wavelet coherence. After matching, we observe an improvement in coherency of RPI records with the Site U1308 record (more areas with larger WTC and constant phase relationship), compared to the original age models (Fig. 9). The improvement is evident in the 10–200 kyr period range where the records have better resolution. In addition, the global correlation coefficients before and after matching for RPI pairs, calculated after interpolation to the age step of the lower resolution record of the pair, all show improvement: from 0.26 to 0.51 for Site 983, 0.26 to 0.47 for Site 984, and 0.29 to 0.43 for Core MD972143. Similarly, we calculate the WTC before and after RPI matching for the isotope record pairs (Fig. 10) to determine whether the RPI matching has disrupted the isotope correlations. The results indicate an improvement for the Site 983 and MD972143 isotope correlations to Site U1308, but a reduction is coherence for the Site 984 to Site U1308 match, particularly for ages >700 ka (Fig. 10). Global correlation coefficients for the isotope correlations to Site U1308 (before and after RPI matching) increase from 0.60 to 0.64 for Site 983, from 0.69 to 0.71 for MD972143, but decrease from 0.59 to 0.58 for Site 984. The low resolution of the isotope record for Site 984 in the 800–1500 ka interval (Fig. 8) may explain the apparent disruption of the correlation of the Site 984 and Site U1308 isotope records after the RPI match.

6. Discussion

The potential of relative paleointensity (RPI) for high-resolution correlation stems from the high rate of change of the Earth's dipole field intensity, that has decreased by ~5% over the last century, and by ~20% over the last 1000 yrs in the archaeological record (Korte and

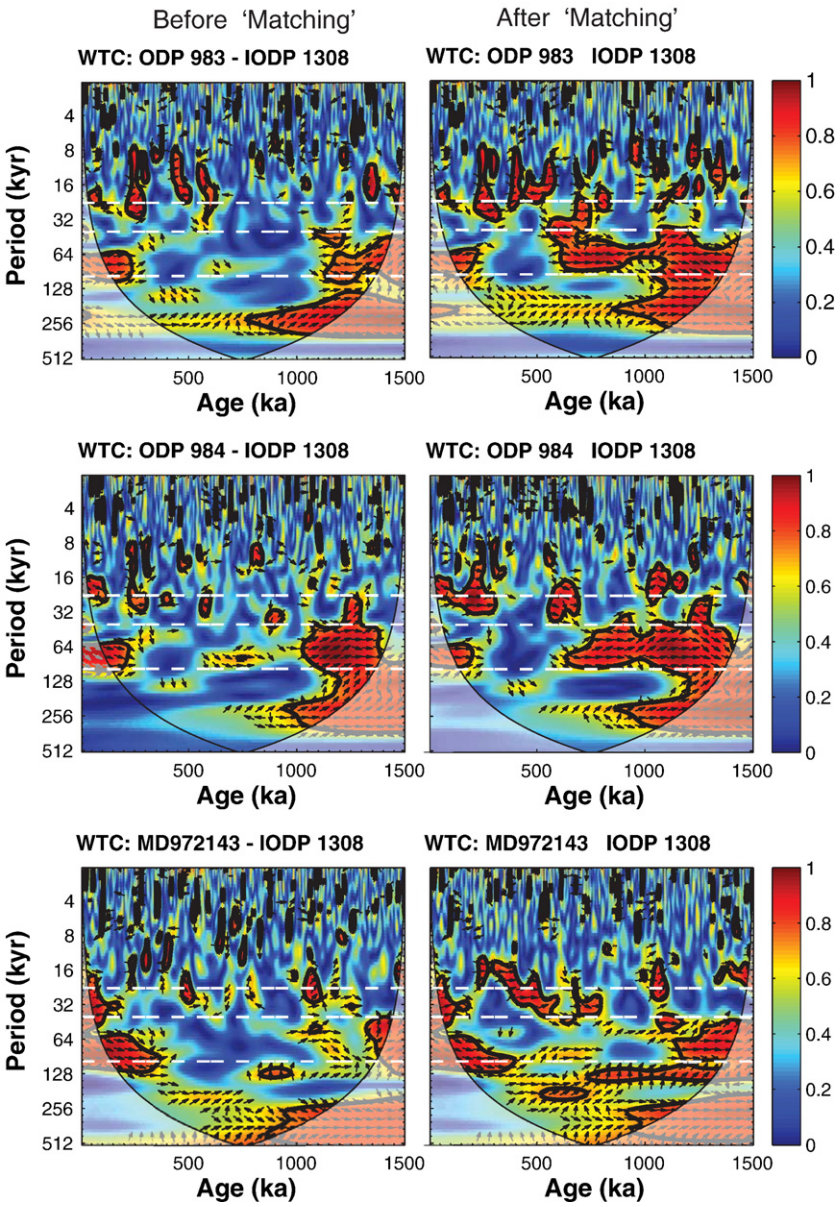

Fig. 9. Squared wavelet coherence (WTC) between paleointensity (RPI) records for IODP Site U1308 and ODP Site 983, ODP Site 984 and Core MD972143, for the original published age models (before matching) and the age models after optimal RPI correlation using the Match protocol (Lisiecki and Lisiecki, 2002). Values of squared wavelet coherence are represented by different colors. The 5% significance level is shown as thick black contour. The cone of influence where edge effects make the analysis unreliable is shown as shaded area. The relative phase relationship is shown as arrows (with in-phase pointing right, anti-phase pointing left). Periods of 100 kyr, 41 kyr and 23 kyr are marked by dashed white lines.

Constable, 2005; Valet et al., 2008). For the last glacial cycle, similarities among RPI proxies from contrasting environments are exemplified by the reasonable correlation of paleointensity stacks for the last 75 kyr (Laj et al., 2000, 2004; Stoner et al., 2002). The similarity of Brunhes-age marine sedimentary RPI records, with paleointensity proxies derived from contrasting archives, for example, from Lake Baikal (Peck et al., 1996) and from the East Pacific Rise deep-tow data (Gee et al., 2000), supports the contention that longer period (>10 kyr) content of sedimentary RPI records is dominated by a global geomagnetic signal. Non-axial-dipole (NAD) components in the historical field vary on centennial timescales (Hulot and Le Mouël, 1994; Hongre et al., 1998; Valet et al., 2008). If similar repeat times hold in the geologic past, paleointensity records from cores with sedimentation rates less than ~15 cm/kyr are unlikely to record anything but the axial dipole field, and therefore should represent a global signal. Although standing non-axial-dipole (NAD) components have been detected in the 5 Myr time-averaged field, their distribution remains controversial and is possibly an artifact of data distribution and selection (Johnson and Constable, 1997; Carlut and Courtillot, 1998) and any effects on RPI records have not been detected. The modulation of cosmogenic isotope flux by geomagnetic field intensity has provided a means for correlating ice-core and marine records, and these correlations also support the contention that RPI variations represent a global signal (e.g. Muscheler et al., 2005). The longer-term (200 kyr) record of ^{10}Be production rate in marine sediments shows inverse correlation with sedimentary RPI records (Frank et al., 1997; Christl et al., 2003; Carcaillet et al., 2003).

The satisfactory match of RPI and benthic isotope data for ODP Sites 983 (60.4°N, 23.6°W) and Site 984 (61.4°N, 24.1°W) have been discussed previously (Channell et al., 2002, 2004; Channell, 1999). These two sites are located in the Iceland Basin on neighboring Gardar (Site 983) and Bjorn (Site 984) sediment drifts, and are separated by 120 km. Comparison of these RPI records with IODP Site 1308 (49.88°N, 24.24°W) provides a test for the comparison of

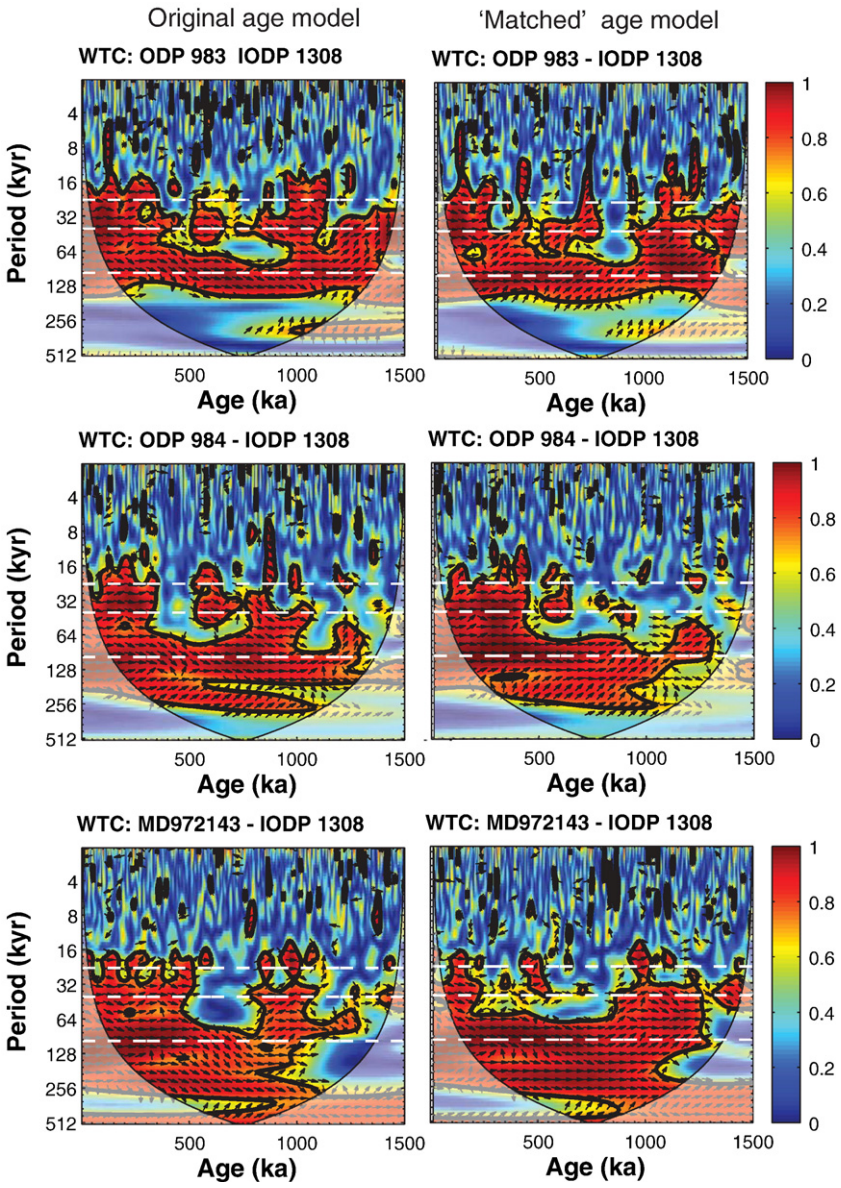

Fig. 10. Squared wavelet coherence (WTC) between benthic oxygen isotope records for IODP Site U1308 and ODP Site 983, ODP Site 984 and Core MD972143, for the original published age models (before matching) and the age models after optimal RPI correlation using the Match protocol (Lisiecki and Lisiecki, 2002). Values of squared wavelet coherence are represented by different colors. The 5% significance level is shown as thick black contour. The cone of influence where edge effects make the analysis unreliable is shown as shaded area. The relative phase relationship is shown as arrows (with in-phase pointing right, anti-phase pointing left). Periods of 100 kyr, 41 kyr and 23 kyr are marked by dashed white lines.

RPI from contrasting depositional environments separated by over 1200 km. The Quaternary sediments from drifts of the Iceland Basin comprise dark gray and greenish gray nannofossil clays with low carbonate (10–30 wt.%). These drift sediments are composed primarily of clastic detritus deposited by bottom currents that sweep southward from the Iceland–Faeroes Ridge, and they do not exhibit distinct glacial–interglacial variations in carbonate concentration. In contrast, the sediments from Site U1308 are marly foraminiferal–nannofossil oozes with distinct glacial–interglacial variations in carbonate concentrations in the 20–95 wt.% range (Expedition 303 Scientists, 2006), reflecting carbonate productivity contrasts related to migration of the polar front. The correlation of the RPI records from ODP Sites 983/984 to Site U1308 is therefore a useful test of the fidelity of RPI proxies, and their ability to record a geomagnetic signal across contrasting depositional environments without debilitating environmental contamination. Similarly, the correlation of the Site U1308 RPI record to a lower sedimentation rate record from the western Pacific (Core MD972143) (Horng et al., 2002, 2003) indicates that the RPI (and benthic isotope) records are dominated by a global signal, attributable (in the case of RPI) to the main axial dipole. The squared wavelet coherence (WTC) provides a means of assessing the improvement in correlation after matching of RPI records, and also allows a measure of the resolution at which coherence can be achieved (~10 kyr for the records considered here). The high-resolution climate archives from pelagic (drift) sites will become increasingly useful through precise global correlation, and the combination of stable isotopes and RPI provides a stratigraphic resolution unlikely to be obtainable using stable isotopes alone.

Acknowledgements

We thank C.-S. Horng and A.P. Roberts for supplying data for Core MD972143. We acknowledge the financial support of the USSSP through the Joint Oceanographic Institutions (now Consortium for Ocean Leadership), and the helpful comments of the journal editor and three journal reviewers.

Appendix A. Supplementary data

Supplementary data associated with this article can be found, in the online version, at doi:10.1016/j.epsl.2008.07.005.

References

Banerjee, S.K., Mellema, J.P., 1974. A new method for the determination of paleointensity from the ARM properties of rocks. Earth Planet. Sci. Lett., 23, 177–184.

Bond, G., Lotti, R., 1995. Iceberg discharges into the North Atlantic on millennial time scales during the last glaciation. Science 267, 1005–1010.

Bond, G., Broecker, W., Johnsen, S., McManus, J., Laberyie, L., Jouzel, J., Bonani, G., 1993. Correlations between climate records from North Atlantic sediments and Greenland ice. Nature 365, 143–147.

Bond, G., Showers, W., Cheseby, M., Lotti, R., Almasi, P., deMenocal, P., Priore, P., Cullen, H., Hajdas, I., Bonani, G., 1997. A pervasive millennial-scale cycle in North Atlantic Holocene and glacial climates. Science, 278, 1257–1266.

Bond, G., Showers, W., Elliot, M., Evans, M., Lotti, R., Hajdas, I., Bonani, G., Johnson, S., 1999. The North Atlantic's 1–2 kyr climate rhythm: relation to Heinrich Events, Dansgaard/Oeschger cycles and the Little ice Age. In: Webb, et al. (Ed.), Mechanisms of Millennial-scale Global Climate Change. Geoph. Monograph Series, vol. 112, pp. 35–58.

Bond, G., Kromer, B., Beer, J., Muscheler, R., Evans, M.N., Showers, W., Hoffmann, S., Lotti-Bond, R., Hajdas, I., Bonani, G., 2001. Persistent solar influence on North Atlantic climate during the Holocene. Science 294, 2130–2136.

Carcaillet, J., Bourles, D.L., Thouveny, N., Arnold, M., 2003. A high resolution authigenic 10Be/9Be record of geomagnetic moment variations over the last 300 ka from sedimentary cores of the Portuguese margin. Earth Planet. Scie. Lett. 6965, 1–16.

Carlut, J., Courtillot, V., 1998. How complex is the time-averaged geomagnetic field over the last 5 million years? Geophys. J. Int. 134, 527–544.

Channell, J.E.T., 1999. Geomagnetic paleointensity and directional secular variation at Ocean Drilling Program (ODP) Site 984 (Bjorn Drift) since 500 ka: comparisons with ODP Site 983 (Gardar Drift). J. Geophys. Res. Solid Earth 104 (B10), 22937–22951.

Channell, J.E.T., Kleiven, H.F., 2000. Geomagnetic palaeointensities and astrochronological ages for the Matuyama–Brunhes boundary and the boundaries of the Jaramillo Subchron: palaeomagnetic and oxygen isotope records from ODP Site 983. Phil. Trans. R. Soc. Lond. A, 358, 1027–1047.

Channell, J.E.T., Raymo, M.E., 2003. Paleomagnetic record at ODP Site 980 (Feni Drift, Rockall) for the past 1.2 Myrs. Geochem. Geophys. Geosyst. 4. doi:10.1029/2002GC000440.

Channell, J.E.T., Hodell, D.A., Lehman, B., 1997. Relative geomagnetic paleointensity and $\delta^{18}O$ at ODP Site 983 (Gardar Drift, North Atlantic) since 350 ka. Earth Planet. Sci. Lett. 153, 103–118.

Channell, J.E.T., Hodell, D.A., McManus, J., Lehman, B., 1998. Orbital modulation of the Earth's magnetic field intensity. Nature 394 (6692), 464–468.

Channell, J.E.T., Mazaud, A., Sullivan, P., Turner, S., Raymo, M.E., 2002. Geomagnetic excursions and paleointensities in the 0.9–2.15 Ma interval of the Matuyama Chron at ODP Site 983 and 984 (Iceland Basin). J. Geophys. Res. 107 (B6). doi:10.1029/2001JB000491.

Channell, J.E.T., Curtis, J.H., Flower, B.P., 2004. The Matuyama–Brunhes boundary interval (500–900 ka) in North Atlantic drift sediments. Geophys. J. Int. 158, 489–505.

Chauvin, A., Roperch, P., Duncan, R.A., 1990. Records of geomagnetic reversals from volcanic islands of French Polynesia, 2-Paleomagnetic study of a flow sequence (1.2 to 0.6 Ma) from the Island of Tahiti and discussion of reversal models. J. Geophys. Res. 95, 2727–2752.

Christl, M., Strobl, C., Mangini, A., 2003. Beryllium-10 in deep-sea sediments: a tracer for the Earth's magnetic field intensity during the last 200,000 years. Quat. Sci. Rev. 22, 725–739.

Clement, B.M., Kent, D.V., 1987. Short polarity intervals within the Matuyama: transition field records from hydraulic piston cored sediments from the North Atlantic. Earth Planet. Sci. Lett. 81, 253–264.

Clement, B.M., Martinson, D.G., 1992. A quantitative comparison of two paleomagnetic records of the Cobb Mountain subchron from North Atlantic deep-sea sediments. J. Geophys. Res. 97, 1735–1752.

Day, R., Fuller, M., Schmidt, V.A., 1977. Hysteresis properties of titanomagnetites: grain-size and compositional dependence. Phys. Earth Planet. Int. 13, 260–267.

Expedition 303 Scientists, Site U1308, 2006. In: Channell, J.E.T., Kanamatsu, T., Sato, T., Stein, R., Alvarez Zarikian, C.A., Malone, M.J. (Eds.), Expedition 303/306 Scientists, Proc. IODP, 303: College Station TX (Integrated Ocean Drilling Program Management International, Inc.). doi:10.2204/iodp.proc.303306.108.2006.

Frank, M., Schwarz, B., Baumann, S., Kubik, P., Suter, M., Mangini, A., 1997. A 200 kyr record of cosmogenic radionuclide production rate and geomagnetic field intensity from ^{10}Be in globally stacked deep-sea sediments. Earth Planet. Sci. Lett., 149, 121–129.

Gee, J.S., Cande, S.C., Hildebrand, J.A., Donnelly, K., Parker, R.L., 2000. Geomagnetic intensityvariations over the past 780 kyr obtained from near-seafloor magnetic anomalies. Nature, 408, 827–832.

Grinsted, A., Moore, J.C., Jevrejeva, S., 2004. Application of the cross wavelet transform and wavelet coherence to geophysical time series. Nonlinear Process. Geophys. 11, 561–566.

Guyodo, Y., Valet, J.-P., 1999. Global changes in intensity of the earth's magnetic field during the past 800 kyr. Nature 399, 249–252.

Guyodo, Y., Richter, C., Valet, J.-P., 1999. Paleointensity record from Pleistocene sediments (1.4-0 Ma) off the California Margin. J. Geophys. Res. 104, 22,953–22,964.

Guyodo, Y., Channell, J.E.T., Thomas, R., 2002. Deconvolution of u-channel paleomagnetic data near geomagnetic reversals and short events. Geophys. Res. Lett. 29 (1845). doi:10.1029/2002GL014963.

Hodell, D.A., Channell, J.E.T., Curtis, J.H., Romero, O.E., Rohl, U., submitted for publication. Onset of "Hudson Strait" Heinrich Events in the eastern North Atlantic at the end of the Middle Pleistocene Transition (~640 ka)? Paleoceanography.

Hongre, L., Hulot, G., Khokhlov, A., 1998. An Analysis of the geomagnetic field over the past 2000 years. Phys. Earth Planet. Inter. 106, 311–335.

Horng, C.S., Lee, M.Y., Pälike, H., Wei, K.-Y., Liang, W.T., Iizuka, Y., Torii, M., 2002. Astronomically calibrated ages for geomagnetic reversals within the Matuyama Chron. Earth Planets Space 54, 679–690.

Horng, C.-S, Roberts, A.P, Liang, W.-T., 2003. A 2.14-Myr astronomically tuned record of relative geomagnetic paleointensity from the western Philippine Sea. J. Geophys. Res. 108, 2059. doi:10.1029/2001JB001698.

Hulot, G., Le Mouël, J.-L., 1994. A statistical approach to the Earth's main magnetic field. Phys. Earth Planet. Int. 82, 167–183.

Johnson, C.L., Constable, C.G., 1997. The time-averaged geomagnetic field: global and regional biases 0–5 Ma. Geophys. J. Int. 131, 643–666.

King, J.W., Banerjee, S.K., Marvin, J., 1983. A new rock-magnetic approach to selecting sediments for geomagnetic paleointensity studies: application to paleointensity for the last 4000 years. J. Geophys. Res. 88, 5911–5921.

Kirschvink, J.L., 1980. The least squares lines and plane analysis of paleomagnetic data. Geophys. J.R. Astr. Soc. 62, 699–718.

Korte, M., Constable, C., 2005. Continuous geomagnetic field models for the past 7 millennia: 2. CALS7K. Geochem. Geophys. Geosyst. 6 (1), Q02H16. doi:10.1029/2004GC000801.

Laj, C., Kissel, C., Mazaud, A., Channell, J.E.T., Beer, J., 2000. North Atlantic palaeointensity stack since 75 ka (NAPIS-75) and the duration of the Laschamp event. Philosophical Transactions—Royal Society. Math. Phys. Eng. Sci. 358, 1009–1025.

Laj, C., Kissel, C., Beer, J., 2004. High resolution global paleointensity stack since 75 kyr (GLOPIS-75) calibrated to absolute values. In: Channell, J.E.T., Kent, D.V., Lowrie, W., Meert, J.G. (Eds.), Timescales of the Paleomagnetic Field. AGU Geophysical Monograph, vol. 145, pp. 255–265.

Levi, S., Banerjee, S.K., 1976. On the possibility of obtaining relative paleointensities from lake sediments. Earth Planet. Sci. Lett. 29, 219–226.

Lisiecki, L.E., Lisiecki, P.A., 2002. The application of dynamic programming to the correlation of paleoclimate records. Paleoceanography 17 (D4), 1049. doi:10.1029/2001PA000733.

Lisiecki, L.E., Raymo, M.E., 2005. A Pliocene–Pleistocene stack of 57 globally distributed benthic delta O-18 records. Paleoceanography 20 (PA1003). doi:10.1029/2004PA001071.

Liu, P.C., 1994. Wavelet spectrum analysis and ocean wind waves. In: F.-G.E., K.P. (Eds.), Wavelets in Geophysics. Academic Press, pp. 151–166.

Mankinen, E.A., Grommé, C.S., 1982. Paleomagnetic data from the Coso Range, California, and current status of the Cobb Mountain normal geomagnetic polarity event. Geophys. Res. Lett. 9, 1239–1282.

Mankinen, E.A., Donnelly, J.M., Grommé, C.S., 1978. Geomagnetic polarity event recorded at 1.1 m.y.b.p. on Cobb Mountain, Clear Lake volcanic field, California. Geology, 6, 653–656.

Martinson, D.G., Menke, W., Stoffa, P., 1982. An inverse approach to signal correlation. J. Geophys. Res. 87, 4807–4818.

Muscheler, R., Beer, J., Kublik, P.W., Synal, H.A., 2005. Geomagnetic field intensity during the last 60,000 years based on ^{10}Be and ^{36}Cl from the Summit ice cores and ^{14}C. Quat. Sci. Rev. 24, 1849–1860.

Peck, J.A., King, J.W., Colman, S.M., Kravchinsky, V.A., 1996. An 84-kyr paleomagnetic record from the sediments of Lake Baikal. J. Geophys. Res. 101, 11365–11385.

Raymo, M.E., Ruddiman, W.F., Backman, J., Clement, B.M., Martinson, D.G., 1989. Late Pliocene variation in Northern Hemisphere ice sheets and North Atlantic deep water circulation. Paleoceanography 4, 413–446.

Ruddiman, W.F., McIntyre, A., Raymo, M., 1986. Matuyama 41,000 year cycles: North Atlantic Ocean and northern hemisphere ice sheets. Earth Planet. Sci. Lett. 80, 117–129.

Ruddiman, W.F., Raymo, M.E., Martinson, D.G., Clement, B.M., Backman, J., 1989. Pleistocene evolution: northern hemisphere ice sheet and north Atlantic ocean. Paleoceanography 4, 353–412.

Shackleton, N.J., Fairbanks, R.G., Chiu, T.-C., Parrenin, F., 2004. Absolute calibration of the Greenland time scale: implications for Antarctic time scales and for $\Delta^{14}C$. Quat. Sci. Rev. 23, 1513–1522.

Singer, B.S., Hoffman, K.A., Chauvin, A., Coe, R.S., Pringle, M.S., 1999. Dating transitionally magnetized lavas of the late Matuyama Chron: toward a new $^{40}Ar/^{39}Ar$ timescale of reversals and events. J. Geophys. Res. 104, 679–693.

Stoner, J.S., Laj, C., Channell, J.E.T., Kissel, C., 2002. South Atlantic (SAPIS) and North Atlantic (NAPIS) geomagnetic paleointensity stacks (0–80 ka): implications for inter-hemispheric correlation. Quat. Sci. Rev. 21, 1141–1151.

Tauxe, L., 1993. Sedimentary records of relative paleointensity of the geomagnetic field: theory and practice. Rev. Geophys. 31, 319–354.

Tauxe, L., LaBrecque, J.L., Dodson, R., Fuller, M., 1983. U-channels—a new technique for paleomagnetic analysis of hydralic piston cores. Trans. Am. Geophys. Union (EOS) 64, 219.

Thomas, R., Guyodo, Y., Channell, J.E.T., 2003. U-channel track for susceptibility measurements. Geochemistry. Geophys. Geosys. (G^3) 1050. doi:10.1029/2002GC000454.

Torrence, C., Compo, G.P., 1998. A practical guide to wavelet analysis. Bulletin of the American Meteorological Society 79 (1), 61–78.

Torrence, C., Webster, P.J., 1999. Interdecadal changes in the ENSO-monsoon system. J. Climate 12 (8), 2679–2690.

Turrin, B.D., Donnelly-Nolan, J.M., Hearn Jr, B.C., 1994. , $^{40}Ar/^{39}Ar$ ages from the rhyolite of Alder Creek, California: age of the Cobb Mountain normal polarity subchron revisited. Geology. 22, 251–254.

Valet, J.-P., Meynadier, L., 1993. Geomagnetic field intensity and reversals during the last four million years. Nature 366, 234–238.
Valet, J.-P., Meynadier, L., Guyodo, Y., 2005. Geomagnetic dipole strength and reversal rate over the past two million years. Nature 435, 802–805.
Valet, J.-P., Herrero-Brevera, E., LeMouel, J.-L., Plenier, G., 2008. Secular variation of the geomagnetic dipole during the past 2000 years. Geochem. Geophys. Geosyst. 9. doi:10.1029/2007GC001728.
Weeks, R., Laj, C., Endignoux, L., Fuller, M., Roberts, A., Manganne, R., Blanchard, E., Goree, W., 1993. Improvements in long-core measurement techniques: applications in palaeomagnetism and palaeoceanography. Geophys. J. Int. 114, 651–662.
Wunsch, C., 2006. Abrupt climate change: an alternative view. Quaternary Research 65, 191–203.
Yamazaki, T., Oda, H., 2005. A geomagnetic paleointensity stack between 0.8 and 3.0 Ma from equatorial Pacific sediment cores. Geochem. Geophys. Geosyst. 6. doi:10.1029/2005GC001001.